ACS APPLIED MATERIALS & INTERFACES

www.acsami.org

Research Article

Reversibly Erasable Broadband Omnidirectional Antireflection Coatings Inspired by Inclined Conical Structures on Blue-Tailed Forest Hawk Dragonfly Wings

Hsin-Yu Tseng, Yu-Han Chen, Ru-Yu Chen, and Hongta Yang*

Cite This: *ACS Appl. Mater. Interfaces* 2020, 12, 10883–10892

Read Online

ACCESS | Metrics & More | Article Recommendations | Supporting Information

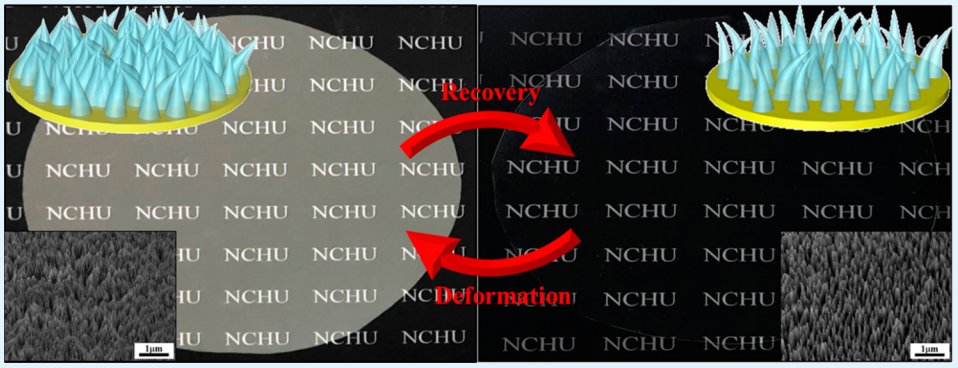

ABSTRACT: Blue-tailed forest hawk dragonfly (*Orthetrum triangulare*) wings, covered with inclined conical structures, are studied for their high transparency and low reflectance for large viewing angles. However, limited by existing technologies, the exquisite inclined structures are not replicated easily or applied adequately. Here, we combine a shear-induced self-assembly approach and a colloidal lithography technology to create omnidirectional antireflection structures that are inspired by dragonfly wings. Nonclose-packed colloid crystals are spin-coated and serve as structural templates in a plasma etching procedure to pattern subwavelength inclined conical structures directly on shape memory polymer-coated substrates. The dependence of the antireflection functionality on the shape and inclination of conical structures is systematically investigated in this research. Compared with a featureless substrate, the structure-covered substrate can display an approximately 8% higher average transmittance in the visible wavelength range at normal incidence and even approximately 23% higher average transmittance as the incident angle increases to 75°. Moreover, the reconfigurable structures composed of shape memory polymers can be repeatedly deformed and recovered as a result of external stimuli at ambient conditions, and the corresponding broadband omnidirectional antireflection functionality is therefore reversibly erased and restored.

KEYWORDS: *dragonfly wings, inclined conical structures, omnidirectional antireflection, shape memory polymers, reversibility*

INTRODUCTION

Owing to high chemical resistance, lightweight, significant degrees of strength, and rapid processability, a variety of optical-grade polymers have taken the place of inorganic optical materials in optical, optoelectronic, and electro-optical applications.[1] Although most polymers exhibit high optical transparency, Fresnel reflectance appears on the polymer surface as light impinges the interface between air and polymer, accompanied by the redistribution of light energy, and thereby degrades the overall performance of optical devices.[2] To reduce glare, protect image readability, and improve optical transmittance of polymer optics, antireflection coatings have been extensively exploited in recent years.[3] On the basis of antireflection principles, single layer antireflection coatings and multilayer antireflection coatings are developed to render destructive interference of reflected light from polymer surfaces.[4,5] However, antireflection coatings suffer from narrow operating wavelengths and incident angles, limited choices of low refractive index coating materials, and performance mismatch between multiple materials.[6]

Over millions of years of evolution, nature has developed various strategies to overcome survival challenges. For example, the hexagonally ordered subwavelength structure arrays on cicada wings, glasswing butterfly wings, and hawk moth wings allow them to avoid tracking by predators.[7−9] The structure arrays build effective refractive index gradients to

Received: January 14, 2020
Accepted: February 7, 2020
Published: February 7, 2020

https://dx.doi.org/10.1021/acsami.0c00823
ACS Appl. Mater. Interfaces 2020, 12, 10883−10892

suppress optical reflectance as well as light scattering on transparent insect wings to overcome the dazzling of insects by light during flight.[10,11] To effectively reduce optical reflectance in the visible light wavelength region, antireflection structures inspired by nature are developed to eliminate the abrupt refractive index change by providing a gradual refractive index transition from air to material surfaces.[12,13] To date, diversified subwavelength structure arrays, including dome arrays, sphere arrays, cone arrays, wire arrays, pillar arrays, and pyramid arrays, have been designed and fabricated for use as antireflection coatings.[14−19] Unfortunately, the broadband antireflection functionality of most structure arrays declines significantly with increasing viewing angles. Unlike many other insects, dragonflies cannot walk with legs and are thus fully dependent on their wings for movement.[20] Interestingly, dragonfly wings possess antireflection ability and the characteristic of superhydrophobicity due to the presence of natural wax-coated irregular structures on these surfaces.[21] Among numerous species of dragonflies, the structures established on the transparent wings of the blue-tailed forest hawk dragonfly (*Orthetrum triangulare*), an Asian freshwater dragonfly species, are far from regular.[22] The randomly inclined conical structures are the origin of a marvelously broadband antireflection functionality for a broad range of incidence angles.[23]

For mimicry of the broadband antireflection performance of the transparent wings, a variety of lithography-based technologies for creating antireflection structures have been reported.[24,25] Nevertheless, most current technologies are restricted to low-resolution subwavelength structures due to surface damage, along with complicated serial processing involved in generating structures. Moreover, it is still challenging to engineer inclined subwavelength structures, which are crucial for improving omnidirectional antireflection performance. By contrast, colloidal lithography has evolved as an alternative for engineering antireflection structure arrays.[26] Self-assembling monolayer colloids are exploited as structural templates in a plasma etching procedure to pattern the material surface. However, most accessible self-assembly technologies are limited by low throughput and consequently are unfeasible in standard microfabrication processes.[27−29] In addition, conventional technologies are available only to self-assemble close-packed colloidal crystals with hexagonal ordering, whereas nonclose-packed arrangements of colloids are preferred for biomimicking the structures on transparent wings.[30] Fueled by the rapid progress of nanotechnologies, Jiang et al. develop a microfabrication-compatible self-assembly technology to deposit nonclose-packed colloidal crystals in a single step.[31] The colloidal crystals can be exploited as structural templates to pattern structure arrays on silicon wafers, which can serve as second-generation templates to fabricate antireflection structures on polymer surfaces.[32] Nevertheless, the soft-lithography replication still encounters difficulty in creating high-resolution features.

Nowadays, reversible antireflection functionality has attracted great attention due to various prospective applications in display screens, optical lenses, sensors, internal partitions, and numerous architectural or vehicle windows.[33] Shape memory polymers are promising candidates for achieving the optical modulation of antireflection in view of the fact that the polymer configurations change in response to external stimuli under different environments.[34] Consequently, the shape memory polymers with structure arrays prospectively promote the development of reversibly erasable antireflection coatings. It is worth noting that external stimuli can be divided into chemical stimuli and physical stimuli. Chemical stimuli alter the intermolecular forces between polymer chains, which can erase and reconstruct the structures.[35,36] However, chemical stimuli generally require the use of specific solvents, which pose environment hazards and potentially dissolve or damage other components in the device. In contrast, physical stimuli, including temperature, lasers, electric fields, and magnetic fields, allow the level of energy sources to be influenced and molecular interactions to be changed, indicating that the structures on the surface can be reversibly switched.[37] For physical stimuli-responsive shape memory polymers, the recovery period is usually long, which significantly impedes many applications that require rapid response.[38] Furthermore, most of the operating length scales of current shape memory polymers are on the order of centimeters, while materials to memorize shape at micrometer-scale are required for largely unexplored applications.

In this work, reversibly erasable shape memory polymer-based antireflection coatings, inspired by blue-tailed forest hawk dragonfly wings, are patterned on polymers by combining a scalable spin-coating technique and a colloidal lithography approach. The shear force-induced self-assembled nonclose-packed colloids can serve as structural templates during plasma etching to engineer inclined conical structure arrays, which display impressive broadband antireflection performance for a wide range of viewing angles. Compared with traditional stimuli-responsive polymers, this new type shape of memory polymer enables instantaneous nanoscopic shape memory recovery by introducing either contact pressures or low surface tension liquids under ambient conditions. The stimuli-responsive shape recovery cycle associated with reversible broadband omnidirectional antireflection functionality considerably improves smart film development. Here, we systematically characterize the antireflection properties of templated inclined conical structure arrays to bridge the gap between bioinspired antireflection design and practical applications.

EXPERIMENTAL SECTION

Reagents and Substrates. The chemicals employed to synthesize spherical silica colloids, including tetraethyl orthosilicate (98 vol %, Sigma-Aldrich), ammonium hydroxide (28 vol %, Sigma-Aldrich), and anhydrous ethanol (200 proof, Sigma-Aldrich), were used without further purification. Deionized water obtained from a Milli-Q Advantage A-10 water purification system exhibits resistivity of 17.5 MΩ·cm at 27 °C and was used directly in all experiments. Ethoxylated trimethylolpropane triacrylate oligomers (ETPTA, SR 415, molecular weight 1176 kDa) and (ethylene glycol) diacrylate oligomers (EGDA, SR 610, molecular weight 742 kDa) were provided by Sartomer Company Corporation. 2-Hydroxy-2-methyl-1-phenyl-1-propanone (Darocur 1173), used as a photoinitiator in the study, was purchased from BASF Corporation. Poly(ethylene terephthalate) (PET) films with a thickness of about 0.01 cm were obtained from Wisegate Technology.

Preparation of Silica Colloid/ETPTA/EGDA Suspensions. Uniform spherical silica colloids with mean diameters of 240, 180, and 90 nm were prepared by the standard StÖber method.[39] In the process, silica colloids are synthesized by hydrolysis of tetraethyl orthosilicate in ethanol solution in which ammonium hydroxide is applied as a catalyst to facilitate the reaction at ambient temperature. The resulting silica colloids are purified using anhydrous ethanol for three centrifugation and dispersion cycles, and then redispersed in a mixture consisting of ETPTA oligomers, EGDA oligomers, and 1 vol

https://dx.doi.org/10.1021/acsami.0c00823
ACS Appl. Mater. Interfaces 2020, 12, 10883−10892

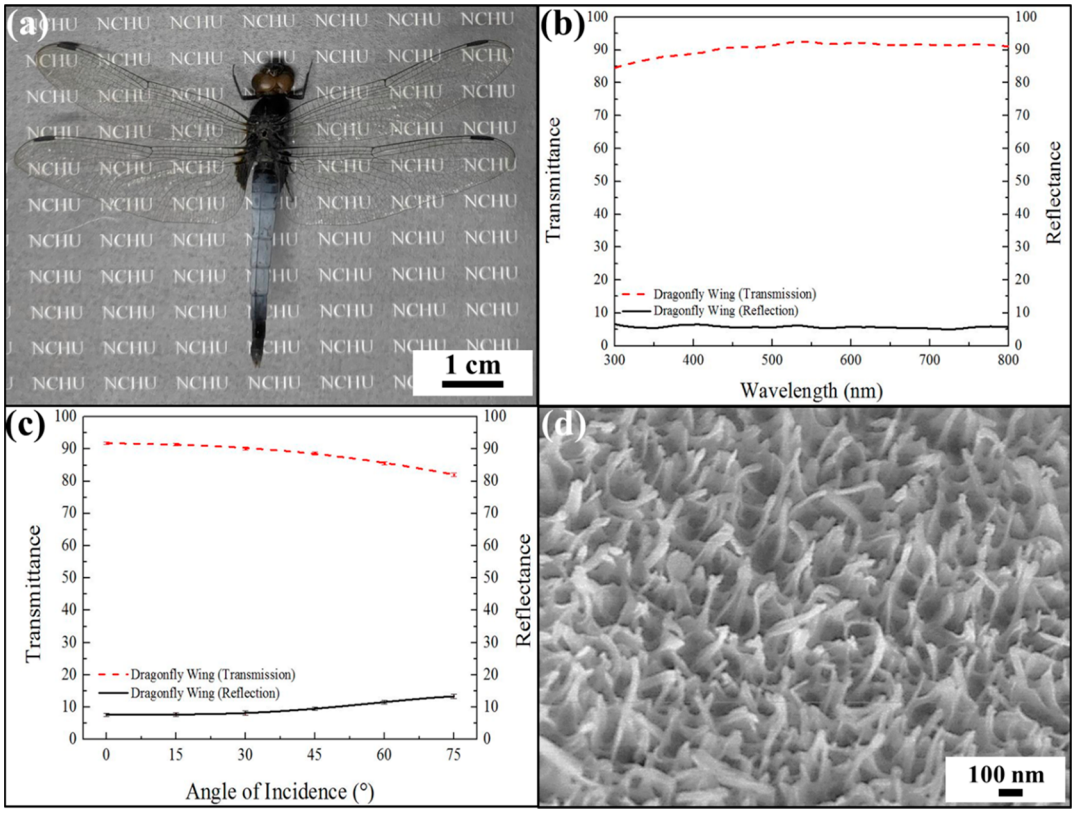

Figure 1. (a) Photograph of a blue-tailed forest hawk dragonfly taken at normal incidence. (b) Optical reflectance and optical transmittance spectra obtained from the dragonfly wing at normal incidence. (c) Optical reflectance and optical transmittance spectra obtained from the dragonfly wing at various incidence angles. The reflectance and transmittance are averaged in a wavelength range from 300 to 800 nm. (d) Side-view SEM image of the dragonfly wing in (a).

% Darocur 1173 by using an ultrasonic homogenizer (Esquire Biotech). The colloid volume fraction of the silica colloidal suspension is controlled at 25 vol %.

Self-Assembly of Silica Colloidal Crystals with Non-Close-Packed Arrangement. A mixture of ETPTA oligomers, EGDA oligomers, and Darocur 1173 is dispensed on a cleaned PET film, which is rinsed with anhydrous ethanol, followed by drying under ambient conditions before use. The oligomer mixture is spin-coated at 3000 rpm for 2 min (WS-400B-6NPP-Lite, Laurell Technologies) and photopolymerized by exposure to UV radiation performed on a UV curing system (X Lite 500 Pulsed UV curing system, OPAS) for 6 s. The prepared silica colloidal suspension is filtered to remove any particle aggregate and deposited on the PETPTA/PEGDA polymer-coated PET film. The coating layer, PETPTA/PEGDA polymer, has shape memory capability. The PET film is slowly tilted to spread the colloidal suspension, followed by spinning at 250 rpm for 1 min, 500 rpm for 1 min, 1200 rpm for 1 min, 3500 rpm for 1 min, 6500 rpm for 1 min, and 8500 rpm for 5 min to remove excess suspension and create two-dimensionally ordered silica colloidal crystals with a nonclose-packed arrangement. After this process, the oligomers are photopolymerized by UV radiation for 6 s.

Fabrication of Shape Memory Conical Structure Arrays. The monolayer silica colloidal crystal/shape memory polymer composite-coated PET film is etched by oxygen and argon reactive ions in an Unaxis Shuttlelock RIE/ICP reactive ion etcher for directly patterning shape memory conical structures on PET substrates. The chamber pressure is 20 mTorr with a fixed oxygen flow rate of 5 SCCM and a fixed argon flow rate of 15 SCCM. The silica structural templates can then be wet etched in an ethanol solution containing hydrofluoric acid (2 vol %) for 3 min and rinsed with anhydrous ethanol.

Characterization. Photographic images of the samples are obtained using a Canon Ixus 185 HS digital camera. The microscopic features and morphologies of the samples are determined by scanning electron microscopy (SEM, JEOL 6335F). The samples are mounted and sputtered with high purity gold using a sputter coater (Agar Sputter Coater) prior to imaging. Optical reflectance and transmittance spectra are obtained by a UV−visible-near-IR spectrometer (Ocean Optics HR4000) with an optical fiber probe (Unice R-400-7-SR) and recorded in the wavelength range from 300 to 800 nm. A halogen-tungsten lamp (Ocean Optics LS-1) is used as the light source.

RESULTS AND DISCUSSION

Blue-tailed forest hawk dragonfly (*Orthetrum triangulare*) wings display high clarity and low haze with white light illumination (Figure 1a). To assess the optical transparency as displayed, the optical reflectance and optical transmittance of dragonfly wings are measured at normal incidence. As disclosed in Figure 1b, the average reflectance is about 7% in the visible wavelength region, whereas the transmittance is about 91% on average, indicating a broadband antireflection characteristic. The antireflection capabilities at various incidence angles are further evaluated (Figure 1c). Apparently, no obvious average reflectance change is observed as the incident angle increases from 0° to 30°, and the average reflectance is increased by about only 6% as the incident angle reaches 75°. The average transmittance spectrum also displays a similar evolution trend as the incident angle varies. The broadband omnidirectional antireflection characteristic originates from inclined conical structures covering the dragonfly wings (Figure 1d).[40] The randomly directed inclined submicrometer-scale conical structures have an average height

https://dx.doi.org/10.1021/acsami.0c00823
ACS Appl. Mater. Interfaces 2020, 12, 10883−10892

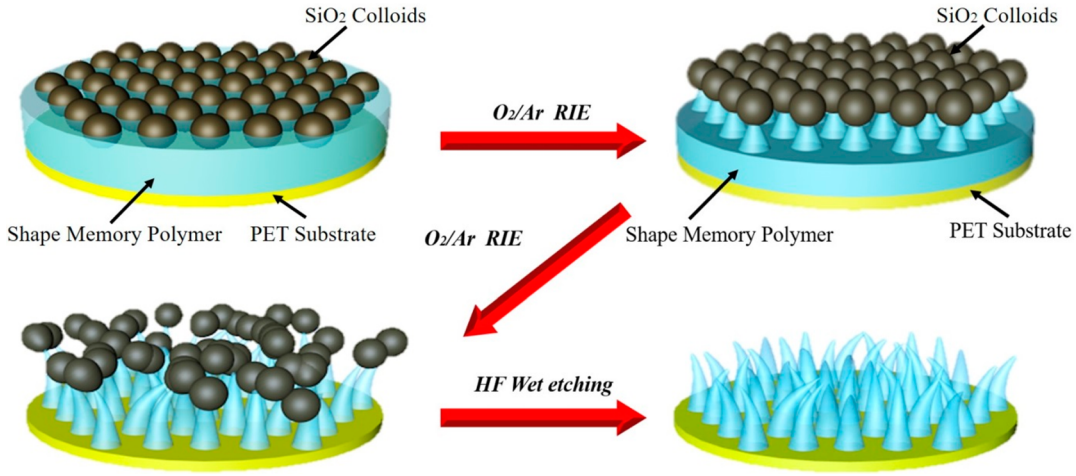

Figure 2. Schematic illustration of the fabrication process for creating dragonfly wing-inspired antireflection coatings.

of about 276 ± 32 nm and remain apart from each other with an average interstructure distance of about 108 ± 41 nm.

Inspired by the broadband omnidirectional antireflection characteristic of blue-tailed forest hawk dragonfly wings, the nonclose-packed inclined conical structures are fabricated through a combination of a shear-induced self-assembly approach and colloidal lithography technology. As illustrated in Figure 2, two-dimensionally ordered nonclose-packed silica colloidal crystals are first spin-coated on a shape memory polymer-coated PET substrate. This simple and scalable self-assembly technology is based on shear-alignment of colloids in the spin-coating process. With the intrinsic nature of high etching selectivity between silica and polymers, the nonclose-packed silica colloids are employed as structural templates during the oxygen and argon RIE treatment for patterning periodic arrays of chess-pawn-like composites consisting of spherical silica tops and conical polymer bottoms. The size and shape of templated polymer bottoms can be adjusted through tuning RIE conditions and templating silica colloid size. It is worth mentioning that the tips of conical polymer bottoms are so thin that they cannot fully support the above silica tops after long RIE treatment, leading to the construction of randomly inclined chess-pawn-like features. The silica tops are then selectively wet etched in an ethanol solution containing 1 vol % hydrofluoric acid to create dragonfly wing-inspired inclined conical structures.

To biomimic the inclined conical structures, a monolayer of 240 nm silica colloid crystals is self-assembled on a shape memory polymer-coated PET substrate. Nonclose-packed arrangement and long-range hexagonal ordering of silica colloids are evident in Figure S1, and the images reveal that the average distance between silica colloids is about 100 nm. In addition, it is observed that the silica colloids float on the surface of the PETPTA/PEGDA coating layer and that the coating layer is much thicker than the diameter of silica colloids. This self-assembly technology is scalable and the periodic domain over the centimeter-scale can be easily achieved.[41] The prepared monolayer nonclose-packed silica colloidal crystal-coated PET substrates are plasma etched by oxygen and argon reactive ions for 5, 7.5, 10, and 12.5 min, respectively. The highly ordered silica colloids can protect the shape memory polymer underneath from being etched.[42] In the etching procedure, the combination of isotropic oxygen plasma etching and anisotropic argon plasma etching leads to the constitution of chess-pawn-like features consisting of spherical silica tops and conical-shaped memory polymer bottoms. The silica tops can then be selectively wet etched in ethanol solution containing hydrofluoric acid to pattern nonclose-packed shape memory polymer conical structures directly on the substrate. The height of conical structures is determined by the plasma etching duration, while the size is predefined by the templating silica colloid size. Figure 3 displays that the conical structures are well-retained and that the long-range hexagonal ordering is preserved during the templating process. Although the shrinkage of spherical silica tops can be neglected during the RIE treatment (Figure S2), the presentation of longer RIE brings about the configuration of higher and sharper conical structures (Figure 3). For RIE durations of 5 and 7.5 min, the resulting conical structures are retained and unbundled after drying of ethanol, whereas the conical structures become too sharp to support the above silica tops as the RIE duration extends to 10 min (Figure S2a), resulting in the inclination of conical structures (Figure 3c). Contrary to commonly observed close-packed structural templates, the nonclose-packed arrangement of silica colloids offers more space to create the inclined structure arrays. It is worth noting that the upper conical structures become sharper and significantly bent with the further increase in RIE duration, leading to serious inclination of chess-pawn-like features (Figure S2b). After wet etching, the resulting conical structures are seriously inclined and form collapsed bundles over large areas as the RIE duration reaches 12.5 min (Figure 3d). The van der Waals forces among adjacent structures with high aspect ratios are also attributed to the observed bundles.[43]

To assess the optical properties of the blue-tailed forest hawk dragonfly wing-inspired inclined conical structure arrays, Figure 3e compares specular reflectance spectra acquired from conical structure arrays with various RIE durations (5, 7.5, 10, and 12.5 min). The featureless PET substrate (black curve) displays an average reflectivity of about 12% in the visible wavelength range at normal incidence, agreeing with previous findings.[44] In contrast, the specular reflectance of conical structure-covered PET substrates decreases over the entire visible spectrum with the increase of RIE duration. Clearly, the conical structures with greater height exhibit smoother refractive index transition and thus reduce normal incidence reflectance more efficiently than the bare PET substrate.[45]

https://dx.doi.org/10.1021/acsami.0c00823
ACS Appl. Mater. Interfaces 2020, 12, 10883−10892

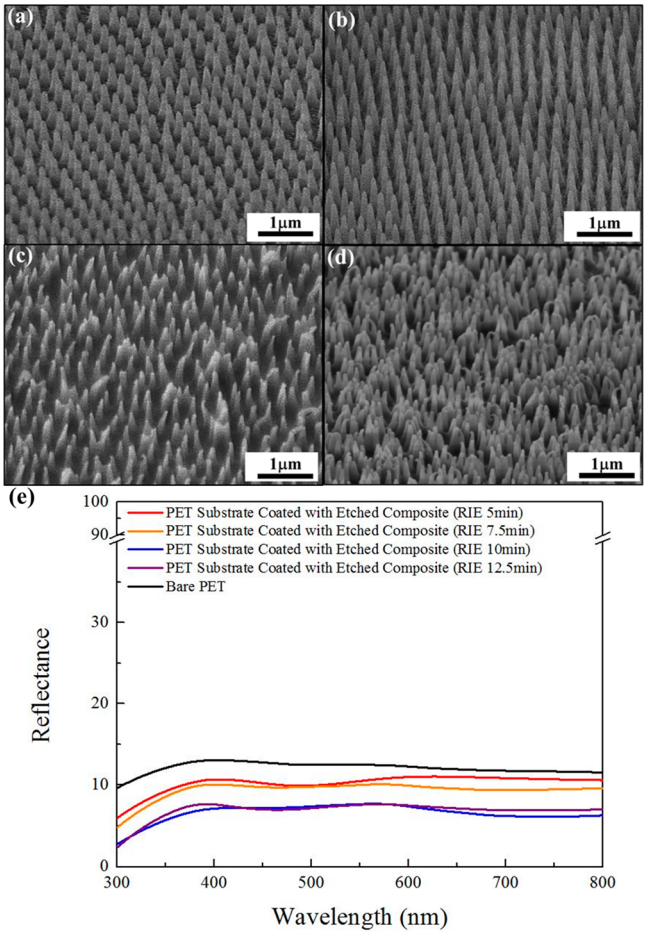

Figure 3. Tilted-view SEM images of the dragonfly wing-inspired conical structures templated from 240 nm silica colloids for different RIE durations of (a) 5 min, (b) 7.5 min, (c) 10 min, and (d) 12.5 min; (e) optical reflectance spectra obtained from a bare PET substrate and PET substrates coated with shape memory polymer conical structures templated from 240 nm silica colloids for different RIE durations at normal incidence.

To investigate the dependence of conical structure shapes on their omnidirectional antireflection performances, the optical reflectance and transmittance spectra of the previously mentioned samples are further evaluated at various incidence angles. As displayed in Figure 4a, for either a flat PET substrate or conical structure-covered PET substrates the average optical reflectance in the visible wavelength region increases as the incident angle increases from 0° to 75°. Moreover, it is found that conical structures with great heights are capable of suppressing optical reflectance even for large incidence angles. It is notable that although the reflectance of the conical structure-covered substrate with 12.5 min RIE treatment remains almost unchanged at large incidence angles, the transmittance of that sample decreases greatly with the increase of incidence angles (Figure 4b). The impaired optical transmittance results from the presented micrometer-scale bundled conical structures with larger scale than the visible wavelengths, as shown in Figure 3c. A portion of the incident visible light is therefore reflected and scattered off of the structures. In contrast, the other average transmittance spectra display similar evolution trends with the average reflectance spectra as the incident angle varies. The transmittances of conical structure-covered substrates increase with RIE duration (5, 7.5, and 10 min) at various incidence angles. Compared with the bare PET substrate, the conical structure-covered substrate with 10 min RIE treatment exhibits about 3% higher average transmittance at 0° (normal incidence) and about 15% higher average transmittance at 75°. Importantly, even though the heights of the inclined conical structures created after 10 min RIE are close to the heights of the conical structures after 7.5 min RIE treatment (Figure 3c,d), the inclined conical structure-covered substrate displays higher transmittances at different incidence angles. The results suggest that broadband omnidirectional antireflection performance can be improved by introducing inclined conical structure arrays on the material surface.

To comprehend the dependence of the shape and inclination of conical structures on the omnidirectional antireflection properties, nonclose-packed 180 nm silica colloidal crystals and nonclose-packed 90 nm silica colloidal crystals are spin-coated on PET substrates for patterning inclined conical structure arrays, respectively (Figure S3 and Figure S4). Figure S5 displays the hexagonally ordered conical structure arrays templated from the 180 nm silica colloidal crystals at various RIE durations, followed by selectively wet etching silica colloids. Obviously, the heights of the resulting conical structures increase with RIE duration, and the structures are bundled and collapsed as the REI duration reaches 10 min. In addition, inclined conical structures are created after 7.5 min RIE treatment. Compared with the

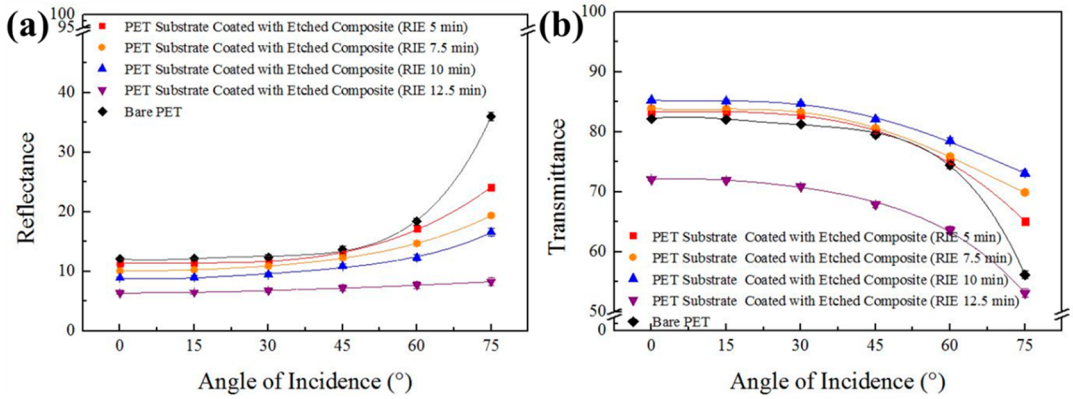

Figure 4. (a) Optical reflectance spectra and (b) optical transmittance spectra obtained from a bare PET substrate and PET substrates coated with shape memory polymer conical structures templated from 240 nm silica colloids for different RIE durations at various incidence angles.

https://dx.doi.org/10.1021/acsami.0c00823
ACS Appl. Mater. Interfaces 2020, 12, 10883−10892

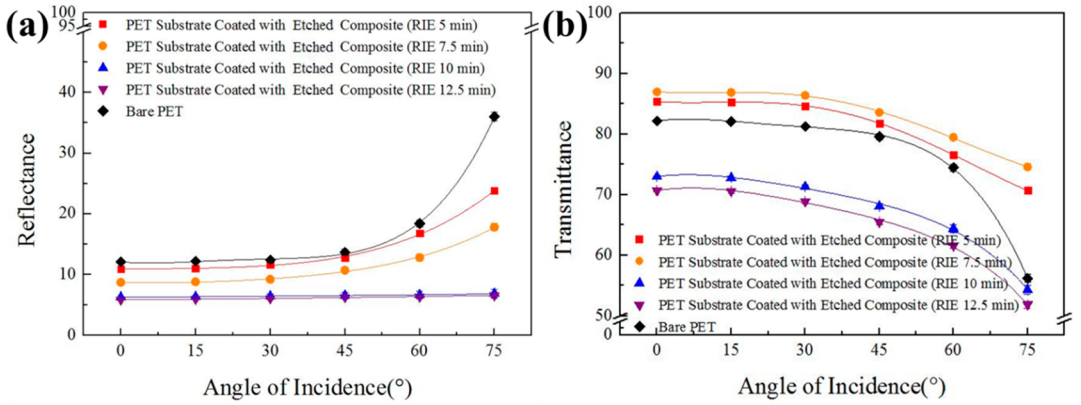

Figure 5. (a) Optical reflectance spectra and (b) optical transmittance spectra obtained from a bare PET substrate and PET substrates coated with shape memory polymer conical structures templated from 180 nm silica colloids for different RIE durations at various incidence angles.

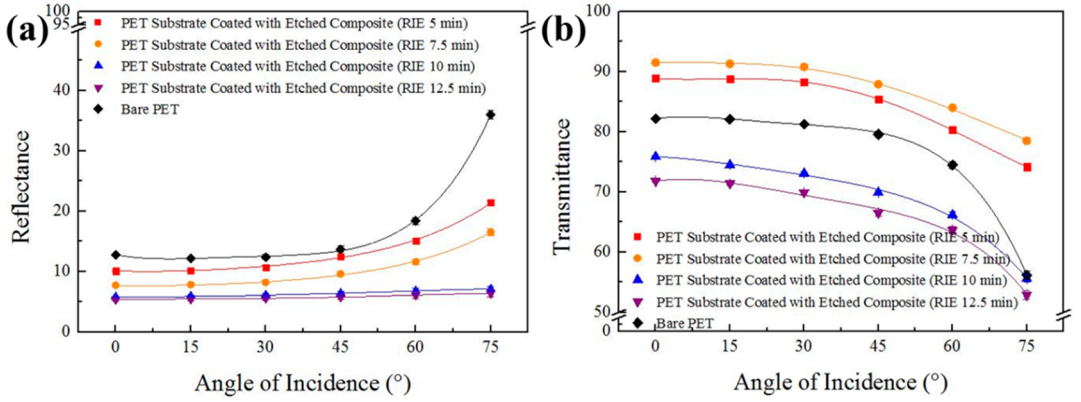

Figure 6. (a) Optical reflectance spectra and (b) optical transmittance spectra obtained from a bare PET substrate and PET substrates coated with shape memory polymer conical structures templated from 90 nm silica colloids for different RIE durations at various incidence angles.

structures as shown in Figure 3, it is evident that shorter structures can be fabricated using smaller templating silica colloids, while the silica colloid size does not significantly affect the shape of the fabricated conical structures. Because the protected region underneath structural templates is proportional to the silica colloid size during the plasma etching procedure, the width of the conical structure base templated from 180 nm silica colloids is smaller than that templated from 240 nm silica colloids.

Spectral reflectance and spectral transmittance of the templated conical structure arrays are evaluated at various incidence angles (Figure 5). Similar to the spectra displayed in Figure 4, the omnidirectional antireflection performance of the conical structure-covered substrates is influenced by RIE duration. The heights of templated conical structures increase with RIE duration, resulting in a smooth refractive index transition at the air and substrate interface. Therefore, the conical structure-covered substrate with longer RIE treatment displays lower reflectivity than that of a bare substrate for the entire visible spectrum at various incidence angles (Figure 5a). Despite that the transmittances of conical structure-covered substrates at 10 min RIE duration and 12.5 min RIE duration significantly decrease as a result of light scattering from bundled and damaged conical structures, the transmittances of the other conical structure-covered substrates (RIE 5 min and RIE 7.5 min) increase with RIE duration (Figure 5b). Compared with a bare substrate, the substrate with 7.5 min RIE exhibits about 5% higher transmittance at 0° and about 19% higher transmittance at 75°. Importantly, even if the shapes of inclined conical structures templated from 180 nm silica colloids with 7.5 min RIE treatment are similar to those templated from 240 nm silica colloids with 10 min RIE treatment (Figure 3c), the structures templated from 180 nm silica colloids exhibit better antireflection performance. This is reasonable because the height and the interstructure spacing of the conical structures templated from 180 nm silica colloids are smaller than visible wavelengths. Hence, less incident visible light is scattered off the conical structure arrays, leading to higher transmittance. Moreover, although the heights of inclined conical structures templated from 180 nm silica colloids with 7.5 min RIE treatment and those templated from 240 nm silica colloids with 7.5 min RIE treatment (Figure 3b) are similar, the structures templated from 180 nm silica colloids display higher transmittance at various incidence angles. The results indicate that omnidirectional antireflection properties can be enhanced by introducing inclined conical structures.

To further improve the transparency of the dragonfly wing-inspired antireflection coatings, 90 nm silica colloidal crystals self-assembled on a PET substrate are utilized to engineer inclined conical structure arrays (Figure S4). Figure S6 shows that inclined conical structures with a height of about 400 nm can be fabricated by applying 7.5 min RIE treatment, whereas the structures are damaged after 10 min RIE. In addition, it is

https://dx.doi.org/10.1021/acsami.0c00823
ACS Appl. Mater. Interfaces 2020, 12, 10883−10892

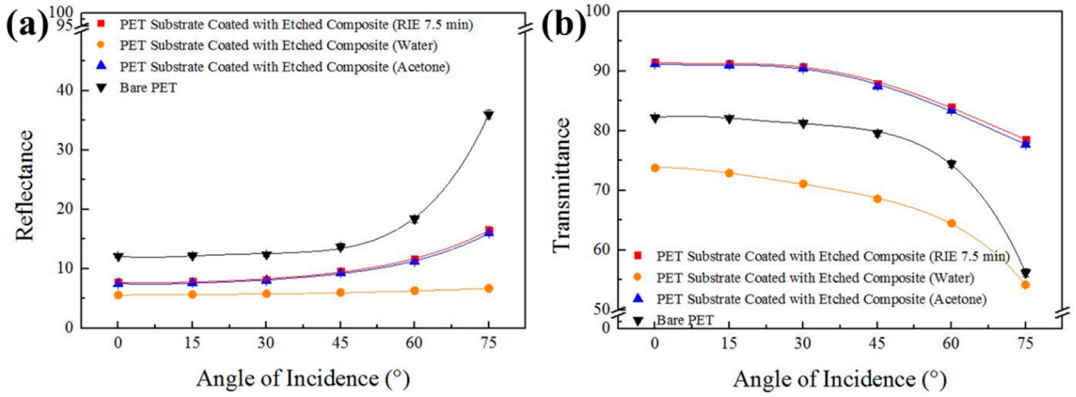

Figure 7. (a) Optical reflectance spectra and (b) optical transmittance spectra obtained from PET substrates coated with shape memory polymer conical structures templated from 90 nm silica colloids with 7.5 min RIE treatment at various incidence angles. The same sample dried out of water, and the water drying sample dried out of acetone are labeled as (water) and (acetone), respectively.

evident that the resulting conical structures are smaller than those templated from 240 nm silica colloids and 180 nm silica colloids. Even though few bundled conical structures are found, the hexagonal ordering of inclined conical structures is apparent.

Figure 6a reveals the optical reflectance spectra of a featureless PET substrate and the conical structure-covered PET substrates at various incidence angles. The reflectance at 0° is decreased from about 12% for a bare substrate to about 7% for the PET substrate covered with conical structure arrays with 7.5 min RIE treatment. Furthermore, the reflectance at 75° can be greatly decreased from about 36% to about 6% by introducing the inclined conical structures. As mentioned previously, the periodic inclined conical structures possess large heights, which can efficiently suppress optical reflectance at different incidence angles by generating a refractive index gradient between air and PET substrate. Additionally, the subwavelength interstructure distance of the conical structures templated from 90 nm silica colloids facilitates efficient suppression of light scattering, and thus incident light propagation is primarily governed by the refractive index gradient of the conical structures. The transmittance spectra in Figure 6b disclose that the average transmittance in the visible wavelength range of this conical structure-covered substrate reaches about 92% at normal incidence and even about 80% as the incident angle increases to 75°. The resulting optical properties agree well with those of blue-tailed forest hawk dragonfly wings, confirming that broadband omnidirectional antireflection characteristics can be achieved by patterning inclined conical structures on material surfaces. In comparison with the optical properties of dragonfly wings (Figure 1c), the conical structure-covered PET substrate templated from 90 nm silica colloids exhibits about 2% higher reflectance and about 2% lower transmittance at 75°. It is worth noting that the structural disordering of inclined conical structures on dragonfly wings may also play a role in developing broadband omnidirectional antireflective properties.

Figure S7 displays the photographs of a bare PET substrate and the inclined conical structure-covered PET substrates templated from 240 nm silica colloids, 180 nm silica colloids, and 90 nm silica colloids. The photographs are taken under white light illumination for viewing angles at 45°. It is obvious that the bare substrate exhibits a milky coloration caused by Fresnel's reflectance of incident light. In contrast to that, the inclined conical structure-covered substrates are less milky, and the letters underneath the substrates are distinctly observed. Additionally, in comparison with the substrates templated from 240 nm silica colloids or 180 nm silica colloids, which exhibit blush coloration resulting from light scattering, the substrate templated from 90 nm silica colloids is macroscopically uniform and highly transparent. These results suggest that large-scale dragonfly wing-inspired broadband antireflection coatings can be engineered through a combination of spin-coating technology with a colloidal lithography approach.

The shape memory polymer used in this study enables the deformation from ordered permanent structures to disordered temporary structures by water evaporation from the templated structures.[46] The recovery of the temporarily deformed structures to the permanent structures can be triggered by applying a contact pressure or drying of low surface tension liquids at room temperature.[47] These unique characteristics of the shape memory polymer provide a platform to achieve reversible antireflection functionality, which is associated with the transition from inclined conical structures to collapsed conical structures (Figure S8).

As demonstrated previously in this research, in comparison with the left featureless PET substrate the right subwavelength inclined conical structure-covered PET substrate exhibits high transparency, resulting from gradual refractive index transition between air and substrate (Figure S9a,b). Interestingly, the transparency of the right substrate disappears, and it becomes translucent after immersion in water, followed by drying of the water under ambient conditions (Figure S9c). The pale white appearance suggests that the conical structures are bundled and collapsed as water evaporates from the structures. This process is a result of the substantial capillary force created by water evaporation, which squeezes the elastic conical structures into disordered arrangements. The surface morphology in Figure S9d further verifies the statements. Surprisingly, the substrate recovers its original inclined conical structures and becomes highly transparent as the substrate is reimmersed in acetone, followed by an acetone drying procedure (Figure S9e,f). From the Young−Laplace equation, it is believed that low surface tension results in a lower capillary force that is not sufficient to squeeze the structures into disordered arrangements.[48] Besides acetone, solvents with low surface tensions, such as ethanol, can also be applied to fully recover the structures by solvent evaporation. In the capillary force-

https://dx.doi.org/10.1021/acsami.0c00823
ACS Appl. Mater. Interfaces 2020, 12, 10883−10892

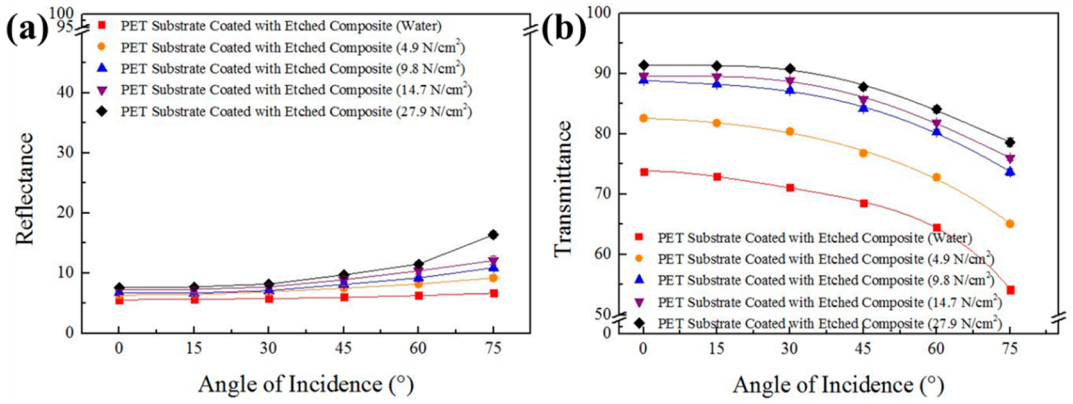

Figure 8. (a) Optical reflectance spectra and (b) optical transmittance spectra obtained from PET substrates coated with shape memory polymer conical structures templated from 90 nm silica colloids with 7.5 min RIE treatment under different pressures at various incidence angles. The same sample dried out of water is labeled as (water).

induced shape memory recovery cycle, the capillary force squeezes the structures, storing excess stresses in the temporarily configured polymer chains. The strained polymer chains exhibit a strong tendency to recover the permanent, stress-free states.

The structure transition and the corresponding antireflection performance can be evaluated by comparing the optical reflectance and transmittance spectra of the samples. In Figure 7, the substrate dried out of water displays low reflectance and transmittance, caused by light scattering from collapsed conical structures, whereas the acetone-recovered substrate covered with inclined conical structures displays impressive broadband omnidirectional antireflection performance. Importantly, the optical spectra of the recovered sample match well with those of the original sample, indicating that the temporarily deformed structures are fully recovered, while the inclined conical structures are triggered by acetone evaporation. More importantly, the recovered antireflection functionality can again be deactivated as the sample is reimmersed in water and then dried out of water. The capillary force-induced shape recovery cycle is reversible and can be repeated for at least 10 cycles (Figure S10).

Even more interesting, the recovery of the inclined conical structures can also be triggered by applying contact forces on the collapsed structures. To verify the feasibility of pressure-induced shape memory recovery, different pressures are applied by placing different weights of a piece of cover glass with a specific area on the collapsed structure-covered substrate. The tilted SEM images in Figure S11 correspond to the structures recovered by applying 0.49 N/cm^2, 0.98 N/cm^2, 1.96 N/cm^2, and 2.94 N/cm and reveal that the temporarily deformed structures are fully recovered to the permanent inclined conical structures as 2.94 N/cm^2 pressure is applied. In contrast, intermediate pressures are capable of inducing only partial recoveries of structures, resulting in fewer bundled conical structures than fully collapsed structures. Although a variety of methodologies have been applied to fabricate pressure-induced tunable structures using elastic materials, the temporarily deformed structures cannot be memorized.[49,50] It is worth noting that higher pressure applied on the substrate leads to the formation of more recovered structures and therefore the shape memory polymer structure-covered substrate under higher applied pressure displays better antireflection performance. The optical reflectance and transmittance spectra of the substrates under different pressures as displayed in Figure 8 further verify these statements. Moreover, the spectra of the structure-covered substrate under 2.94 N/cm^2 pressure are consistent with the spectra of the untreated structure-covered substrate (Figure 6). The agreement indicates that the broadband omnidirectional antireflection characteristics of deformed structures can be fully recovered by applying pressures. As demonstrated previously, the recovered antireflection functionality can be erased by capillary force generated by water evaporation. The pressure-induced shape recovery cycle is reversible and can be repeated for at least 10 cycles (Figure S12).

CONCLUSIONS

In summary, stimuli-responsive antireflection structures are directly fabricated on polymer substrates through a combination of scalable colloidal self-assembly technology and colloidal lithography technology. The resulting inclined conical structures, inspired by blue-tailed forest hawk dragonfly wings, exhibit high transparency and impressive broadband antireflection performance for wide viewing angles. Importantly, the capillary force generated from water evaporation induces deformed conical structure bundles, leading to the pale white appearance. Simultaneously, the recovery of the temporarily deformed structures to the inclined conical structures can be evoked by drying the structures of low surface tension liquids or applying contact pressure at room temperature. The repeatable stimuli-responsive shape recovery cycle associated with the reversible broadband omnidirectional antireflection functionality offers a wide spectrum of promising applications in optical devices.

ASSOCIATED CONTENT

Supporting Information

The Supporting Information is available free of charge at https://pubs.acs.org/doi/10.1021/acsami.0c00823.

SEM images of nonclose-packed silica colloidal crystals on a shape memory polymer-coated PET substrate fabricated by spin-coating technology. SEM images, photographic images, and reversible antireflection functionality of PET substrates coated with dragonfly wing-inspired conical structures by applying solvent and pressure stimulation. Schematic illustration of the

https://dx.doi.org/10.1021/acsami.0c00823
ACS Appl. Mater. Interfaces 2020, 12, 10883−10892

reversible mechanism for the antireflection functionality (PDF)

AUTHOR INFORMATION

Corresponding Author

Hongta Yang − *Department of Chemical Engineering, National Chung Hsing University, Taichung City 40227, Taiwan;* orcid.org/0000-0002-5822-1469; Email: hyang@dragon.nchu.edu.tw

Authors

Hsin-Yu Tseng − *Department of Chemical Engineering, National Chung Hsing University, Taichung City 40227, Taiwan*

Yu-Han Chen − *Department of Chemical Engineering, National Chung Hsing University, Taichung City 40227, Taiwan*

Ru-Yu Chen − *Department of Chemical Engineering, National Chung Hsing University, Taichung City 40227, Taiwan*

Complete contact information is available at: https://pubs.acs.org/10.1021/acsami.0c00823

Notes

The authors declare no competing financial interest.

ACKNOWLEDGMENTS

Acknowledgment is made to the National Science Council (Grants MOST107-2221-E-005-035, MOST 108-2221-E-005-040, and MOST 108-2221-E-005-038-MY2) for financial support of this research.

REFERENCES

(1) Ouyang, X.; Yin, Z.; Wu, J.; Zhou, C.; Zhang, A. P. Rapid Optical μ-printing of Polymer Top-Lensed Microlens Array. *Opt. Express* **2019**, *27*, 18376−18382.

(2) Tsai, T.-Y.; Lee, Z.-C.; Tsao, H.-X.; Lin, S.-T. Minimization of Fresnel Reflection by Anti-reflection Fiber Bragg Grating Inscribed at the Fiber Ends. *Opt. Express* **2019**, *27*, 11510−11515.

(3) Chi, F. T.; Liu, D. J.; Wu, H. Y.; Lei, J. H. Mechanically Robust and Self-cleaning Antireflection Coatings from Nanoscale Binding of Hydrophobic Silica Nanoparticles. *Sol. Energy Mater. Sol. Cells* **2019**, *200* (8), 109939.

(4) Willey, R. R. Understanding Key Design Principles of Antireflection Coatings. *Laser Focus World* **2016**, *52*, 31−35.

(5) Bacon-Brown, D. A.; Braun, P. V. Tunable Antireflection Coating to Remove Index-Matching Requirement for Interference Lithography. *Adv. Opt. Mater.* **2018**, *6*, 1701049.

(6) Moayedfar, M.; Assadi, M. K. Various Types of Anti-reflective Coatings (ARCS) Based on the Layer Composition and Surface Topography: A Review. *Rev. Adv. Mater. Sci.* **2018**, *53*, 187−205.

(7) Gupta, A.; Cheng, H. Y.; Lin, K. H.; Wu, C. T.; Roy, P. K.; Ghosh, S.; Chattopadhyay, S. Gold Coated Cicada Wings: Anti-Reflective Micro-Environment for Plasmonic Enhancement of Fluorescence from Upconversion Nanoparticles. *Mater. Sci. Eng., C* **2019**, *102*, 569−577.

(8) Huang, Y. F.; Chattopadhyay, S.; Jen, Y. J.; Peng, C. Y.; Liu, T. A.; Hsu, Y. K.; Pan, C. L.; Lo, H. C.; Hsu, C. H.; Chang, Y. H.; Lee, C. S.; Chen, K. H.; Chen, L. C. Improved Broadband and Quasi-omnidirectional Anti-reflection Properties with Biomimetic Silicon Nanostructures. *Nat. Nanotechnol.* **2007**, *2*, 770−774.

(9) Siddique, R. H.; Gomard, G.; Holscher, H. The Role of Random Nanostructures for the Omnidirectional Anti-reflection Properties of the Glasswing Butterfly. *Nat. Commun.* **2015**, *6*, 8.

(10) Nakamura, M.; Mano, I.; Taniguchi, J. Fabrication of Micro-lens Array with Antireflection Structure. *Microelectron. Eng.* **2019**, *211*, 29−36.

(11) Chaliyawala, H.; Purohit, Z.; Khanna, S.; Ray, A.; Pati, R.; Mukhopadhyay, I. Effective Light Polarization Insensitive and Omnidirectional Properties of Si Nanowire Arrays Developed on Different Crystallographic Planes. *Nanotechnology* **2019**, *30*, 124002.

(12) Fan, Y.; Chen, J.; Ma, D. Enhancement of Light Extraction of Green Top-emitting Organic Light-emitting Diodes with Refractive Index Gradually Changed Coupling Layers. *Org. Electron.* **2013**, *14*, 3234−3239.

(13) Spiller, E.; Haller, I.; Feder, R.; Baglin, J.; Hammer, W. Graded-Index AR Surfaces Produced by Ion Implantation on Plastic Materials. *Appl. Opt.* **1980**, *19*, 3022−3026.

(14) Grandidier, J.; Deceglie, M. G.; Callahan, D. M.; Atwater, H. A. Simulations of Solar Cell Absorption Enhancement Using Resonant Modes of a Nanosphere Array. *Proc. SPIE* **2012**, *2*, 825603.

(15) Xu, H. B.; Lu, N.; Qi, D. P.; Gao, L. G.; Hao, J. Y.; Wang, Y. D.; Chi, L. F. Broadband Antireflective Si Nanopillar Arrays Produced by Nanosphere Lithography. *Microelectron. Eng.* **2009**, *86*, 850−852.

(16) Wang, Y.; Lu, N.; Xu, H.; Shi, G.; Xu, M.; Lin, X.; Li, H.; Wang, W.; Qi, D.; Lu, Y. Biomimetic Corrugated Silicon Nanocone Arrays for Self-cleaning Antireflection Coatings. *Nano Res.* **2010**, *3*, 520−527.

(17) Grandidier, J.; Deceglie, M. G.; Callahan, D. M.; Atwater, H. A. Simulations of Solar Cell Absorption Enhancement Using Resonant Modes of a Nanosphere Array. *J. Photonics Energy* **2012**, *2*, No. 024502.

(18) Putnam, M. C.; Boettcher, S. W.; Kelzenberg, M. D.; Turner-Evans, D. B.; Spurgeon, J. M.; Warren, E. L.; Briggs, R. M.; Lewis, N. S.; Atwater, H. A. Si Microwire-Array Solar Cells. *Energy Environ. Sci.* **2010**, *3*, 1037−1041.

(19) Kumar, M. D.; Kim, H.; Kim, J. Periodically Patterned Si Pyramids for Realizing High Efficient Solar Cells by Wet Etching Process. *Sol. Energy* **2015**, *117*, 180−186.

(20) Wang, X.; Song, W.; Li, Z.; Cong, Q. Fabrication of Superhydrophobic AAO-Ag Multilayer Mimicking Dragonfly Wings. *Chin. Sci. Bull.* **2012**, *57*, 4635−4640.

(21) Aideo, S. N.; Mohanta, D. Limiting Hydrophobic Behavior and Relectance Response of Dragonfly and Damselfy Wings. *Appl. Surf. Sci.* **2016**, *387*, 609−616.

(22) Han, Z.; Wang, Z.; Feng, X.; Li, B.; Mu, Z.; Zhang, J.; Niu, S.; Ren, L. Antireflective Surface Inspired from Biology: A Review. *Biosurf Biotribol.* **2016**, *2*, 137−150.

(23) Chen, Y.-C.; Huang, Z.-S.; Yang, H. Cicada-Wing-Inspired Self-cleaning Antireflection Coatings on Polymer Substrates. *ACS Appl. Mater. Interfaces* **2015**, *7*, 25495−25505.

(24) Su, W. X.; Wu, C. Y.; Lee, Y. C. Anti-reflection Nano-structures Fabricated on Curved Surface of Glass Lens Based on Metal Contact Printing Lithography. *Microelectron. Eng.* **2019**, *214*, 15−20.

(25) Cai, J.; Qi, L. Recent Advances in Antireflective Surfaces Based on Nanostructure Arrays. *Mater. Horiz.* **2015**, *2*, 37−53.

(26) Yu, B.; Cong, H. L.; Yang, Z.; Yang, S. J.; Wang, Y. Z.; Zhai, F.; Wang, Y. F. Preparation of Humidity-Sensitive Poly(ethylene glycol) Inverse Opal Micropatterns Using Colloidal Lithography. *Materials* **2017**, *10*, 1035.

(27) Gasvoda, R. J.; van de Steeg, A. W.; Bhowmick, R.; Hudson, E. A.; Agarwal, S. Surface Phenomena During Plasma-Assisted Atomic Layer Etching of SiO_2. *ACS Appl. Mater. Interfaces* **2017**, *9*, 31067−31075.

(28) Liu, Y.; Peng, X. C.; Wang, Z. D.; Zhang, T.; Yu, Y.; Zou, J. J.; Deng, W. J.; Zhu, Z. F. Inductively Coupled Plasma Etching of the GaAs Nanowire Array Based on Self-Assembled SiO2 Nanospheres. *Jpn. J. Appl. Phys.* **2019**, *58*, 010908.

(29) Zhang, L. J.; Horantner, M. T.; Zhang, W.; Yan, Q. F.; Snaith, H. J. Near-Neutral-Colored Semitransparent Perovskite Films Using a Combination of Colloidal Self-Assembly and Plasma Etching. *Sol. Energy Mater. Sol. Cells* **2017**, *160*, 193−202.

(30) Li, Y.; Zhang, J.; Yang, B. Antireflective Surfaces Based on Biomimetic Nanopillared Arrays. *Nano Today* **2010**, *5*, 117−127.

(31) Yu, S.; Dong, S.; Jiao, X.; Li, C.; Chen, D. Ultrathin Photonic Polymer Gel Films Templated by Non-Close-Packed Monolayer

Colloidal Crystals to Enhance Colorimetric Sensing. *Polymers* **2019**, *11*, 534.
(32) Choi, K.; Yoon, Y.; Jung, J.; Ahn, C. W.; Lee, G. J.; Song, Y. M.; Ko, M. J.; Lee, H. S.; Kim, B.; Kang, I. S. Super-Antireflective Structure Films with Precisely Controlled Refractive Index Profile. *Adv. Opt. Mater.* **2017**, *5*, 6.
(33) Jang, H. J.; Kim, Y. J.; Yoo, Y. J.; Lee, G. J.; Kim, M. S.; Chang, K. S.; Song, Y. M. Double-Sided Anti-reflection Nanostructures on Optical Convex Lenses for Imaging Applications. *Coatings* **2019**, *9*, 404.
(34) Jiang, H.; Kelch, S.; Lendlein, A. Polymers Move in Response to Light. *Adv. Mater.* **2006**, *18*, 1471−1475.
(35) Kumpfer, J. R.; Rowan, S. J. Thermo-, Photo-, and Chemo-Responsive Shape-Memory Properties from Photo-Cross-Linked Metallo-Supramolecular Polymers. *J. Am. Chem. Soc.* **2011**, *133*, 12866−12874.
(36) Fang, Y.; Ni, Y.; Choi, B.; Leo, S. Y.; Gao, J.; Ge, B.; Taylor, C.; Basile, V.; Jiang, P. Chromogenic Photonic Crystals Enabled by Novel Vapor-Responsive Shape-Memory Polymers. *Adv. Mater.* **2015**, *27*, 3696−3704.
(37) Leng, J.; Lan, X.; Liu, Y.; Du, S. Shape-Memory Polymers and Their Composites: Stimulus Methods and Applications. *Prog. Mater. Sci.* **2011**, *56*, 1077−1135.
(38) Zhao, W.; Liu, L.; Zhang, F.; Leng, J.; Liu, Y. Shape Memory Polymers and Their Composites in Biomedical Applications. *Mater. Sci. Eng., C* **2019**, *97*, 864−883.
(39) Stöber, W.; Fink, A.; Bohn, E. Controlled Growth of Monodisperse Silica Spheres in the Micron Size Range. *J. Colloid Interface Sci.* **1968**, *26*, 62−69.
(40) Hooper, I. R.; Vukusic, P.; Wootton, R. Detailed Optical Study of the Transparent Wing Membranes of the Dragonfly Aeshna Cyanea. *Opt. Express* **2006**, *14*, 4891−4897.
(41) Ren, L. J.; Liu, H. K.; Wu, H.; Hu, M. B.; Wang, W. Toward Cluster Materials with Ordered Structures via Self-Assembly of Heterocluster Janus molecules. *Adv. Mater.* **2020**, *32*, 1805863.
(42) Zhang, M.; Watson, P. *Reactive Ion Etching Selectivity of Si/SiO_2: Comparing of Two Fluorocarbon Gases CHF_3 and CF_4*; Singh Center for Nanotechnology, 2019.
(43) Wei, Z.; Schneider, T. M.; Kim, J.; Kim, H.-Y.; Aizenberg, J.; Mahadevan, L. Elastocapillary Coalescence of Plates and Pillars. *Proc. R. Soc. London, Ser. A* **2015**, *471*, 20140593.
(44) Lin, C.-Y.; Lin, K.-Y. A.; Yang, T.-W.; Chen, Y.-C.; Yang, H. Self-Assembled Hemispherical Nanowell Arrays for Superhydrophobic Antireflection Coatings. *J. Colloid Interface Sci.* **2017**, *490*, 174−180.
(45) Boden, S. A.; Bagnall, D. M. Tunable Reflection Minima of Nanostructured Antireflective Surfaces. *Appl. Phys. Lett.* **2008**, *93*, 133108.
(46) Fox, C. H.; Ter Hurrne, G. M.; Wojtecki, R. J.; Jones, G. O.; Horn, H. W.; Meijer, E.; Frank, C. W.; Hedrick, J. L.; García, J. M. Supramolecular Motifs in Dynamic Covalent PEG-Hemiaminal Organogels. *Nat. Commun.* **2015**, *6*, 7417.
(47) Fang, Y.; Leo, S.-Y.; Ni, Y.; Wang, J.; Wang, B.; Yu, L.; Dong, Z.; Dai, Y.; Basile, V.; Taylor, C. Reconfigurable Photonic Crystals Enabled by Multistimuli-Responsive Shape Memory Polymers Possessing Room Temperature Shape Processability. *ACS Appl. Mater. Interfaces* **2017**, *9*, 5457−5467.
(48) Gregg, S.; Sing, K. W. *Adsorption, Surface Area and Porosity*; Academic Press: London, 1982; pp 195−197.
(49) Fang, Y.; Ni, Y.; Leo, S.-Y.; Taylor, C.; Basile, V.; Jiang, P. Reconfigurable Photonic Crystals Enabled by Pressure-Responsive Shape-Memory Polymers. *Nat. Commun.* **2015**, *6*, 7416.
(50) Fang, Y.; Ni, Y.; Leo, S.-Y.; Wang, B.; Basile, V.; Taylor, C.; Jiang, P. Direct Writing of Three-Dimensional Macroporous Photonic Crystals on Pressure-Responsive Shape Memory Polymers. *ACS Appl. Mater. Interfaces* **2015**, *7*, 23650−23659.

https://dx.doi.org/10.1021/acsami.0c00823
ACS Appl. Mater. Interfaces 2020, 12, 10883−10892